Supplementary Materials

Synthesis of metal-phenanthroline-modified hypercrosslinked polymer for enhanced CO_2 capture and conversion via chemical and photocatalytic methods under ambient conditions

Huang Ouyang[1,#], Mengjie Peng[1,#], Kunpeng Song[2], Shengyao Wang[3], Hui Gao[1], Bien Tan[1,*]

[1]Key Laboratory of Material Chemistry for Energy Conversion and Storage, Ministry of Education, Hubei Key Laboratory of Material Chemistry and Service Failure, School of Chemistry and Chemical Engineering, Huazhong University of Science and Technology, Wuhan 430074, Hubei, China.

[2]College of Chemistry and Chemical Engineering, China West Normal University, Nanchong 637009, Sichuan, China.

[3]College of Science, Huazhong Agricultural University, Wuhan 430070, Hubei, China.

[#]Authors contributed equally.

[*]**Correspondence to:** Prof. Bien Tan, Key Laboratory of Material Chemistry for Energy Conversion and Storage, Ministry of Education, Hubei Key Laboratory of Material Chemistry and Service Failure, School of Chemistry and Chemical Engineering, Huazhong University of Science and Technology, Luoyu Road No. 1037, Wuhan 430074, Hubei, China. E-mail: bien.tan@mail.hust.edu.cn

Characterizations

Fourier transform infrared (FT-IR) spectra of the solid were obtained by using a Bruker VERTEX 70 FT-IR spectrometer with the KBr disk method. UV-Visible absorption spectra of the polymers were measured on a Shimadzu UV-2600 UV-Vis spectrometer by measuring the reflectance of powders in the solid state. Solid-state ^{13}C cross-polarization magic-angle spinning (CP/MAS) NMR spectra were recorded on a WB 400 MHz Bruker Avance II spectrometer and collected on a 2.5 mm double-resonance MAS probe with a spinning rate of 20 kHz. The products of the CO_2 conversion reaction were identified by ^{1}H NMR spectra using a Bruker AV400 instrument in $CDCl_3$. The field-emission scanning electron microscopy (FE-SEM) images were recorded on an FEI Sirion 200 field-emission scanning electron microscope operated at 10 kV. The high-resolution transmission electron microscopy (HR-TEM) images and elemental mapping were undertaken on a TalosF200x microscope (FEI Corp. Holland). Co content data was determined by Inductively Coupled Plasma Optical Emission Spectrometer (ICP-OES) on an ICP-OES 730 (Agilent Corp. USA). The elemental analysis (EA) was performed over an organic elemental analyzer i.e., Vario Micro Cube. Thermogravimetric analysis (TGA) was performed from room temperature to 800 °C with a PerkinElmer Instrument Pyris1 TGA under nitrogen. The X-ray photoelectron spectroscopy (XPS) measurements were carried out on a Krato AXIS-ULTRA DLD-600 photoelectron spectrograph. Gas sorption properties were measured by employing a Micromeritics ASAP2020 surface area and porosity analyzer. Prior to each cycle experiment, the samples were degassed at 120 °C for 8 h. CO_2 sorption isotherms were measured on a Micromeritics ASAP 2020 analyzer. The procedure was repeated over several cycles. Isotope-labelling experiment for CO_2 reduction was performed using HCP-PNTL-Ni-B powder (10 mg), acetonitrile, water and triethanolamine (3:1:1 vol. mixture, 5 mL) and sealed with a septum. The resulting suspension was ultrasonicated for 5 minutes and then purged with $^{13}CO_2$ for 5 min. The reaction mixture was illuminated with a 300 W Xe light source equipped with a $\lambda > 420$ nm cut-off filter. The gas-phase was analyzed by using a gas chromatography (Agilent GC-MS 7890B) with a mass-spectrometer (Agilent GC-MS 5977B) equipped with a GC-CARBONPLOT column (60 m length, 0.32 mm inner diameter).

Synthesis procedure

Synthesis of PNTL-A[1]: At room temperature, 3,8-dibromo-1,10-phenanthroline (3.0 mmol, 1.01 g), (3,5-diphenylphenyl)boronic acid (7.5 mmol, 2.05 g), and anhydrous potassium carbonate (K_2CO_3, 30.0 mmol, 4.14 g) were accurately weighed in a 100 mL three-neck flask, followed by the addition of 15 mL deionized water and 30 mL 1,4-dioxane as the solvent. After bubbling with nitrogen for 30 min, $Pd(PPh_3)_4$ (0.3 mmol, 0.36 g) was added, followed by continuous stirring at 100 °C for 48 h. Then cooling to room temperature, deionized water was added to quench the reaction, and the organic layer was collected by extraction with dichloromethane. The filtered solution was dried with anhydrous magnesium sulfate, and the filtrate was obtained. The solid product was obtained by rotary evaporation of the filtrate and subjected to three rounds of recrystallization in N,N-Dimethylformamide. The resulting filter cake was dried at 60 °C in a vacuum oven for 24 h to obtain a white solid, with a yield of approximately 33%. ^{1}H NMR (400 MHz, $CDCl_3$) 0.91-0.98 (m, 24 H), 1.30-1.60 (m, 32 H), 1.78 (m, 4 H), 3.94 (m, 8 H), 7.05 and 7.67 (AA´BB´, 16 H, 7.83 (dd, 2 H, J = 1.5), 7.87 (d, 4 H, J = 1.5),7.98 (s, 2H), 8.58 (s, 2 H), and 9.60 (s, 2 H).

Synthesis of PNTL-B[2]: PNTL-B was synthesized using the same procedures as that of PNTL-A except (3,5-diphenylphenyl)boronic acid was replaced by (4-(9H-carbazol-9-yl)phenyl)boronic acid. Yield: 41%. ^{1}H NMR (400 MHz, DMSO-d_6) 9.70 (s, 2H), 9.07-9.06 (d, 2H), 8.41-8.37 (m, 8H), 8.28 (s, 2H), 7.99-7.96 (d, 4H), 7.64-7.56 (m, 8H), 7.46-7.41 (t, 4H).

Catalysis protocol

General Process for CO_2 Cycloaddition of Epoxides. Various amounts of epoxides (25 mmol), catalyst (20 mg), and Bu_4NBr were added into a 20 mL stainless autoclave with a 10 mL Teflon-lined container. CO_2 gas was filled and vented three times to ensure the complete filling of CO_2 in the stainless autoclave. The reaction was conducted at 0.1 MPa at 25 °C with continuous stirring for the desired time. The product was dissolved in ethyl acetate and the insoluble solid was pelleted by centrifugation. Using 1,3,5-trimethylbenzene as an internal standard, the conversion and selectivity were determined by gas chromatography (GC). The cyclic carbonate was evaluated by ^1H NMR spectroscopy. After the first cycle, ethanol and ethyl acetate mixture were added for catalyst precipitation, and the mixture was centrifuged to separate all the insoluble materials. The residue was further dried for 24 hours at 60 °C before its use in the following cycle. The recyclability test was repeated several times.

Carbon Dioxide Reduction Experiments. A quartz flask was charged with the HCP-PNTL-M-B powder (10 mg), ($[Ru(bpy)_3Cl_2]\cdot 6H_2O$, 10 mg), acetonitrile, water, and triethanolamine (TEOA) (3:1:1 vol mixture, 20 mL) and sealed. The resulting suspension was ultrasonicated for 5 min and then purged with CO_2 for 15 min. The reaction mixture was illuminated with a 300 W Xe light source (perfect light) equipped with $\lambda > 420$ nm cutoff filter. Gaseous product was acquired with gas-tight syringe and analyzed on Shimadzu GC-2014 gas chromatograph equipped with ShinCarbon ST micropacked column (Restek 80 - 100 mesh, 2 m length, and 0.53 mm inner diameter) and thermal conductivity detector calibrated against standard gas mixtures of known concentration. Isotope-labeling $^{13}CO_2$ reduction test was performed under the same condition mentioned above andCO_2 was fully replaced by $^{13}CO_2$. The gas product was analyzed by gas chromatography (Agilent 7890B GC) with mass spectrometer (Agilent 5977B MS) equipped with GCCARBONPLOT column (60 m length, 0.32 mm inner diameter).

Supplementary Table 1. Elemental analysis of HCP-PNTL and HCP-PNTL-Co

Sample	C %	H %	N %
HCP-PNTL-A	69.0	4.8	3.1
HCP-PNTL-Co-A	68.6	4.7	2.9
HCP-PNTL-B	68.7	4.8	5.7
HCP-PNTL-Co-B	68.1	4.5	5.6

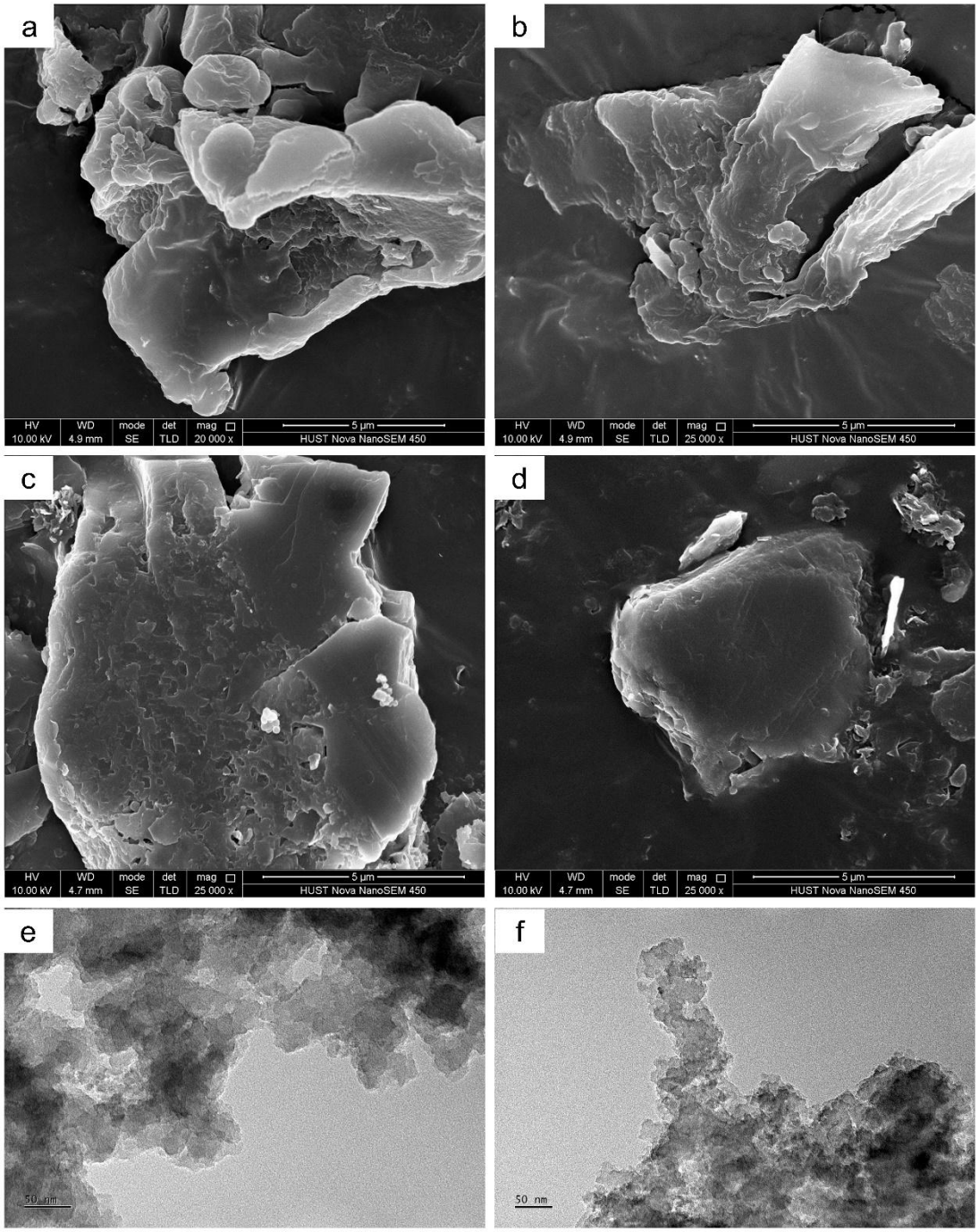

Supplementary Figure 1. FE-SEM images of (a) HCP-PNTL-A, (b) HCP-PNTL-Co-A, (c) HCP-PNTL-B and (d) HCP-PNTL-Co-B; HR-TEM images of (e) HCP-PNTL-Co-A and (f) HCP-PNTL-Co-B.

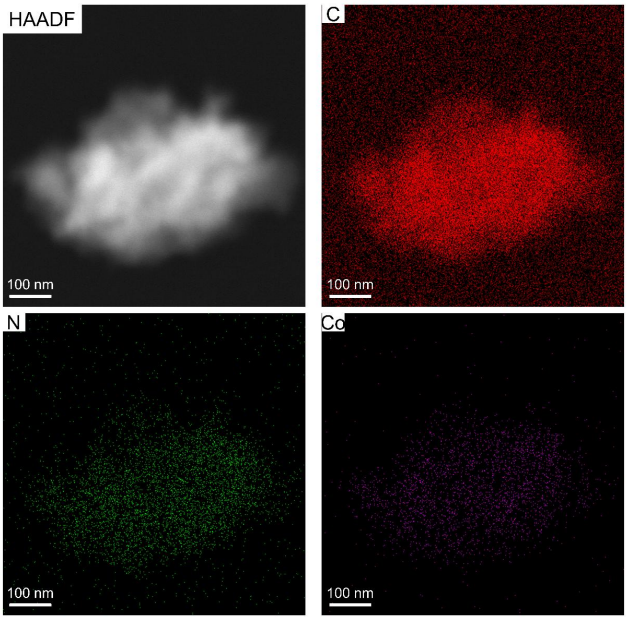

Supplementary Figure 2. HADDF-STEM and mapping images of HCP-PNTL-Co-A.

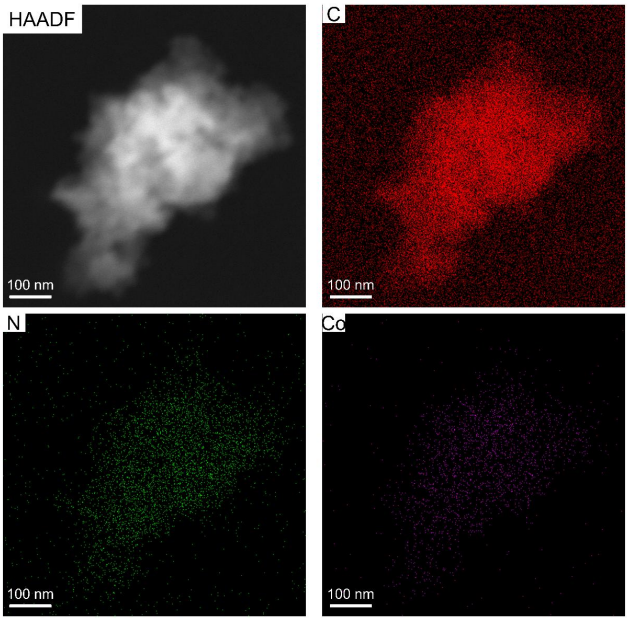

Supplementary Figure 3. HADDF-STEM and mapping images of HCP-PNTL-Co-B.

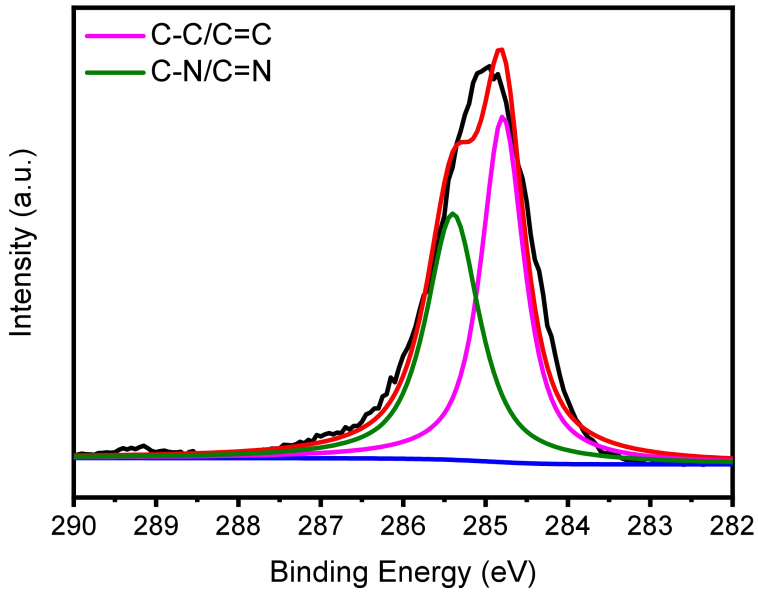

Supplementary Figure 4. XPS spectra for C1s of HCP-PNTL-A.

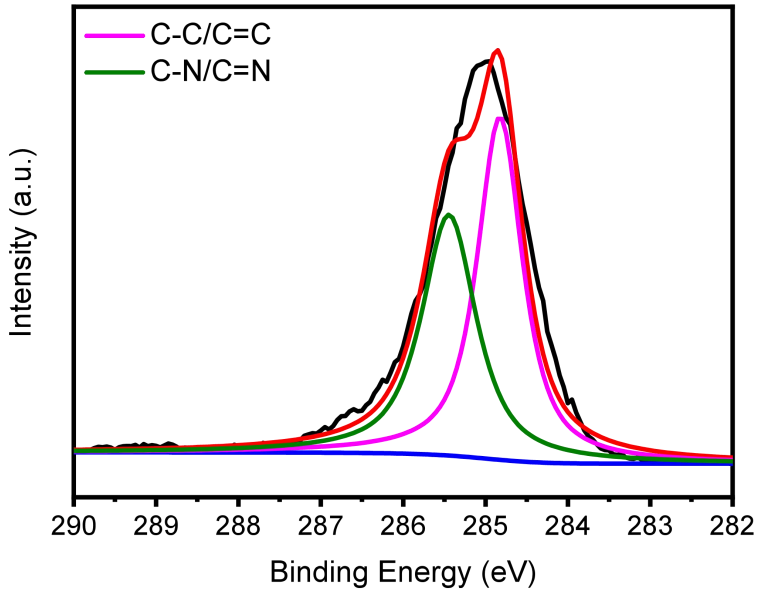

Supplementary Figure 5. XPS spectra for C1s of HCP-PNTL-B.

Supplementary Table 2. The structural parameters of HCP-PNTL and HCP-PNTL-Co

Sample	N %	Co^{2+} wt%[a]	S_{BET}[b] (m^2 g^{-1})	S_L[c] (m^2 g^{-1})	PV[d] (cm^3 g^{-1})	MPV[e] (cm^3 g^{-1})	CO_2 uptake[f] (wt%)/(mmol/g)	CO_2 uptake[g] (wt%)/(mmol/g)	Qst[h] (kJ mol^{-1})
HCP-PNTL-A	3.1	-	951	1413	0.60	0.22	14.0 /3.2	8.5/1.9	27.5
HCP-PNTL-Co-A	2.9	1.5	609	929	0.44	0.13	9.8/2.2	6.3/1.4	30.3
HCP-PNTL-B	5.7	-	475	693	0.30	0.13	9.7/2.2	6.6/1.5	31.4
HCP-PNTL-Co-B	5.6	1.3	147	225	0.20	0.03	8.9/2.0	5.5/1.3	33.0

[a]The content of metal Co^{2+} in the polymer was characterized by ICP-OES. [b]Surface area calculated from nitrogen adsorption isotherms at 77 K using the BET equation. [c]Surface area calculated from nitrogen adsorption isotherms at 77 K using the Langmuir equation. [d]Pore volume calculated from the nitrogen isotherm at $P/P_0 = 0.995$ and 77 K. [e]Micropore volume calculated from nitrogen isotherm at $P/P_0 = 0.050$. [f]Volumetric CO_2 uptake measured with a Micromeritics ASAP 2020 M analyzer at 1 bar and 273 K. [g]Volumetric CO_2 uptake measured with a Micromeritics ASAP 2020 M analyzer at 1 bar and 298 K. [h]Isosteric heat of adsorption of polymers determined volumetrically using a Micromeritics ASAP 2020 M analyzer at 273 and 298 K.

Supplementary Table 3. The catalytic performance for chemical conversion of CO_2 cycloaddition with PO over various catalytic systems

Catalyst	T (°C)	P (MPa)	Time (h)	Yield (%)	TON (TOF h^{-1})	Ref.
P-POF-Zn	120	3	2.5	99	3323 (1329)	[3]
Co/POP-TPP	29	0.1	24	96	432 (18)	[4]
HUST-1-Co	25	0.1	48	95	3101 (64)	[5]
Cu/POP-Bpy	29	0.1	48	99	192 (4)	[6]
Zn/TPA-TCIF(BD)	40	0.5	10	99	2900 (290)	[7]
Co-CMP	25	0.1	48	82	168 (4)	[8]
Mg-Por/DVB@POPs	30	0.1	48	9	1800 (38)	[9]
PPS⊂COF-TpBpy-Cu	25	0.1	72	94	94 (1)	[10]
COF-salen-Co	25	0.1	144	96	3744 (26)	[11]
Co-MON	60	1	12	75	1500 (125)	[12]
Zn/HAzo-POP-1	25	0.1	48	99	202 (4)	[13]
Bp-Zn@MA	100	1	1.5	99	3378 (2252)	[14]
HCP-PNTL-Co-A	25	0.1	48	75	3681 (77)	This work
HCP-PNTL-Co-B	25	0.1	48	95	5380 (112)	This work

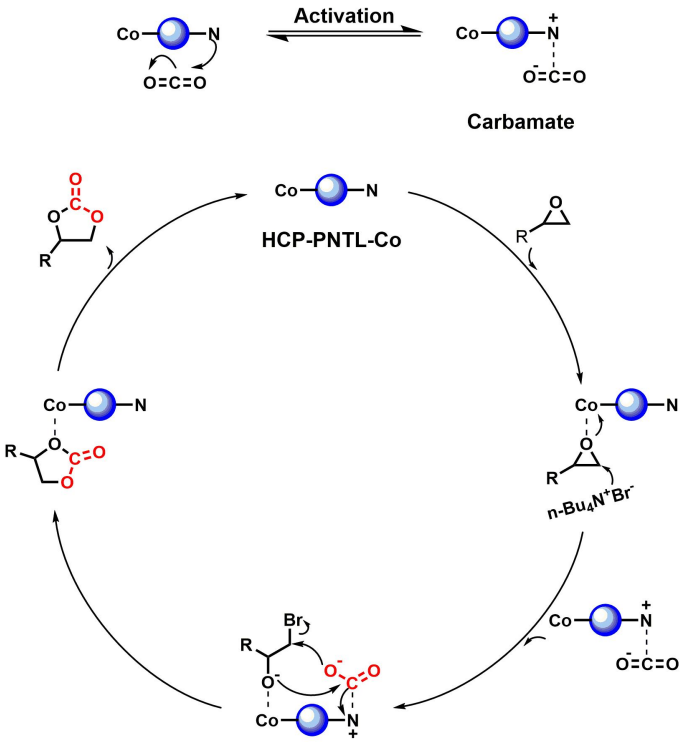

Supplementary Figure 6. The possible mechanism for CO_2 cycloaddition catalyzed by HCP-PNTL-Co.

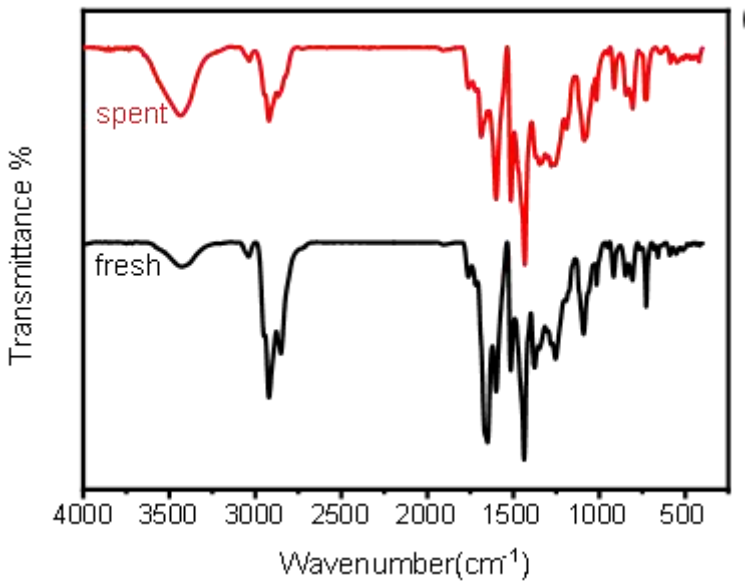

Supplementary Figure 7. FT-IR spectra of HCP-PNTL-Co-B before and after recycling.

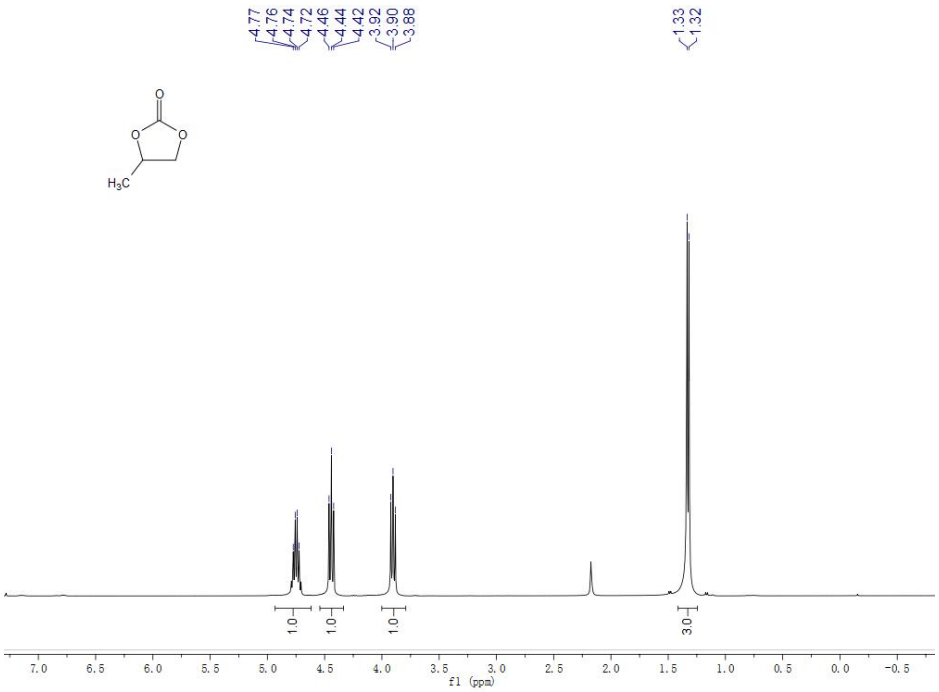

Supplementary Figure 8. ^{1}H NMR spectrum of 4-methyl-1,3-dioxolan-2-one.

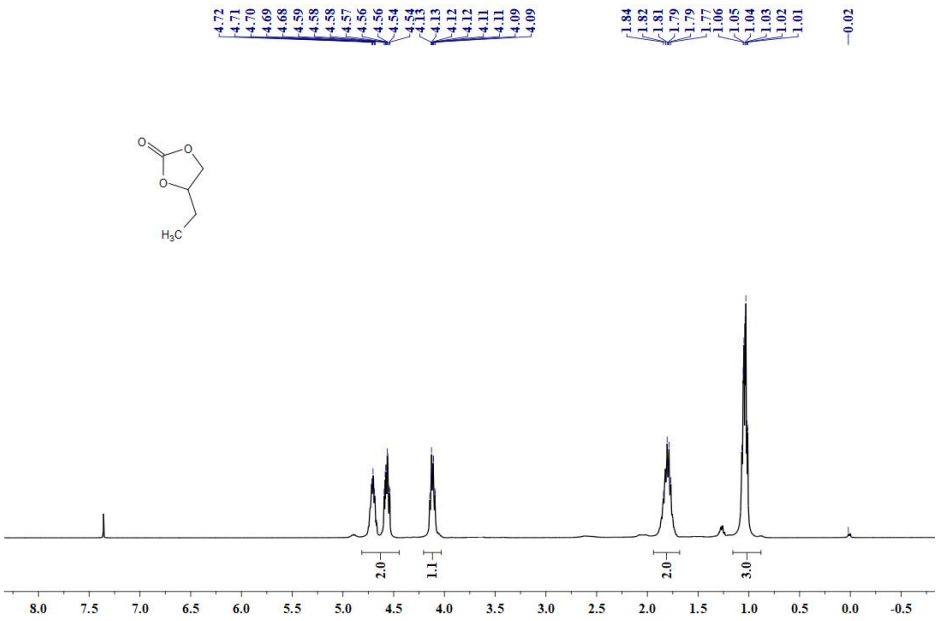

Supplementary Figure 9. ^{1}H NMR spectrum of 4-ethyl-1,3-dioxolan-2-one.

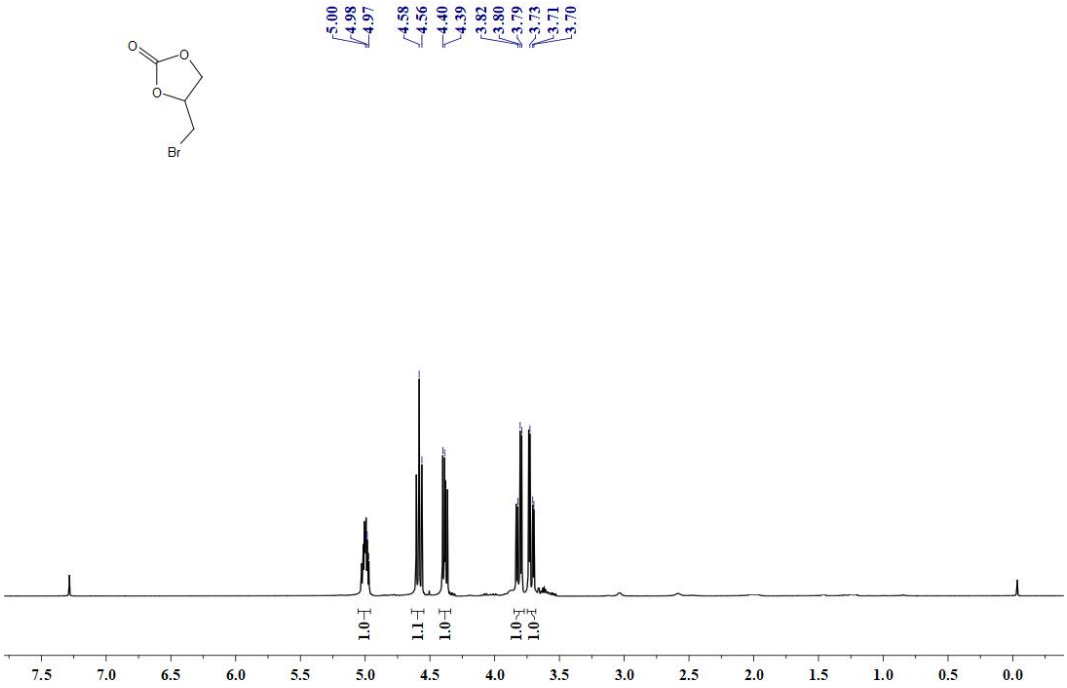

Supplementary Figure 10. ^{1}H NMR spectrum of 4-(bromomethyl)-1,3-dioxolan-2-one.

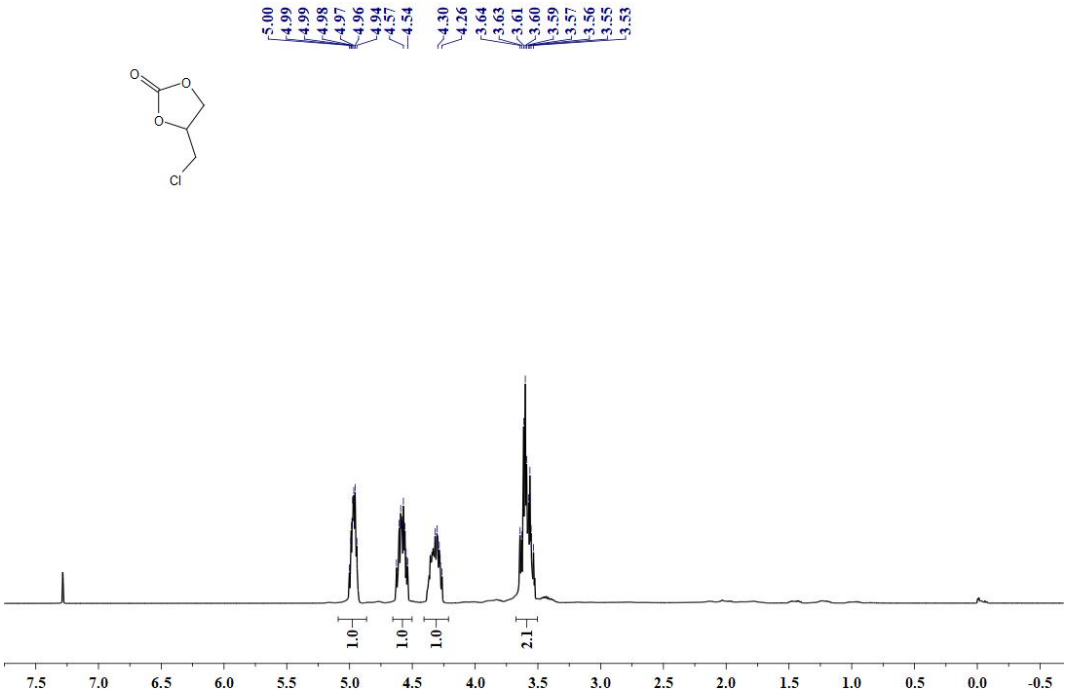

Supplementary Figure 11. ^{1}H NMR spectrum of 4-(chloromethyl)-1,3-dioxolan-2-one.

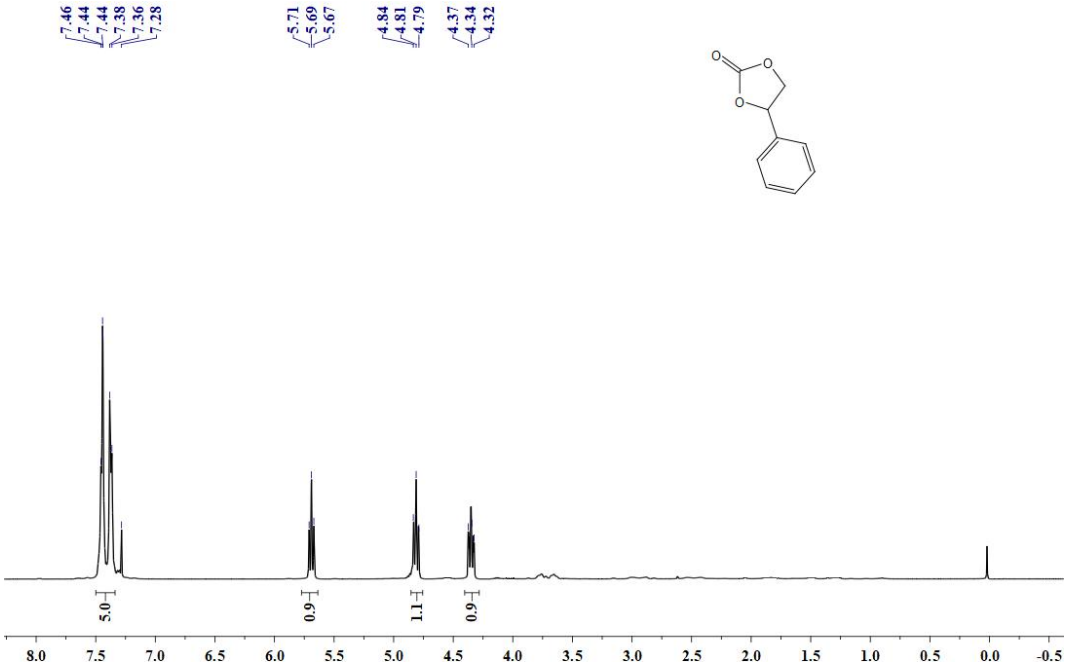

Supplementary Figure 12. ^{1}H NMR spectrum of 4-phenyl-1,3-dioxolan-2-one.

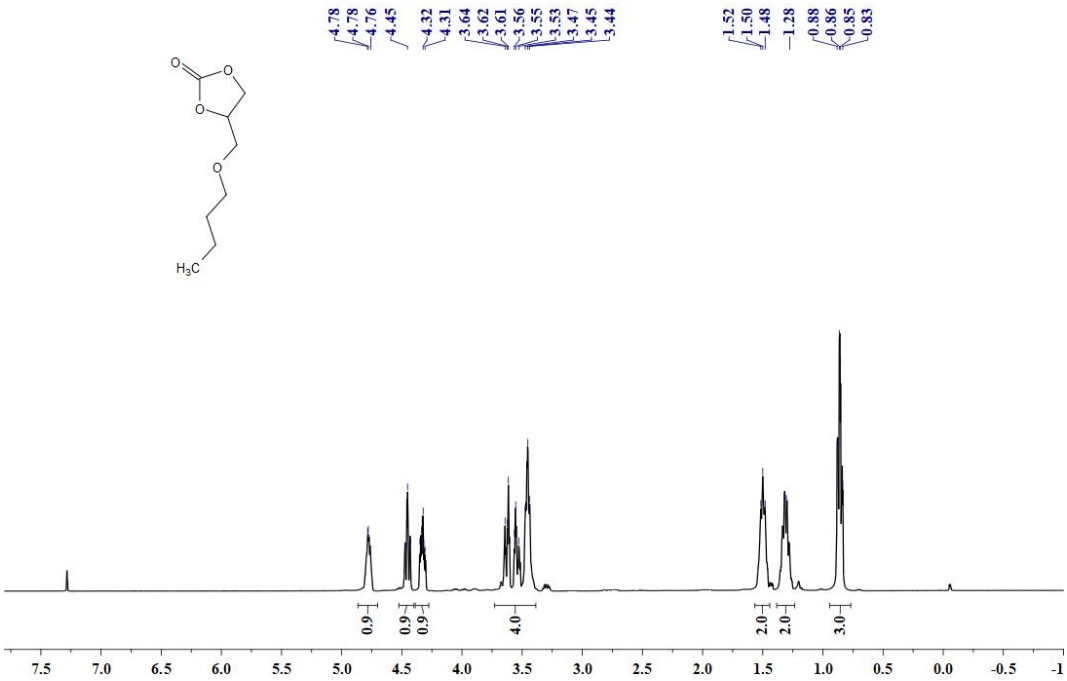

Supplementary Figure 13. ^{1}H NMR spectrum of 1,2-epoxy-3-butoxypropane.

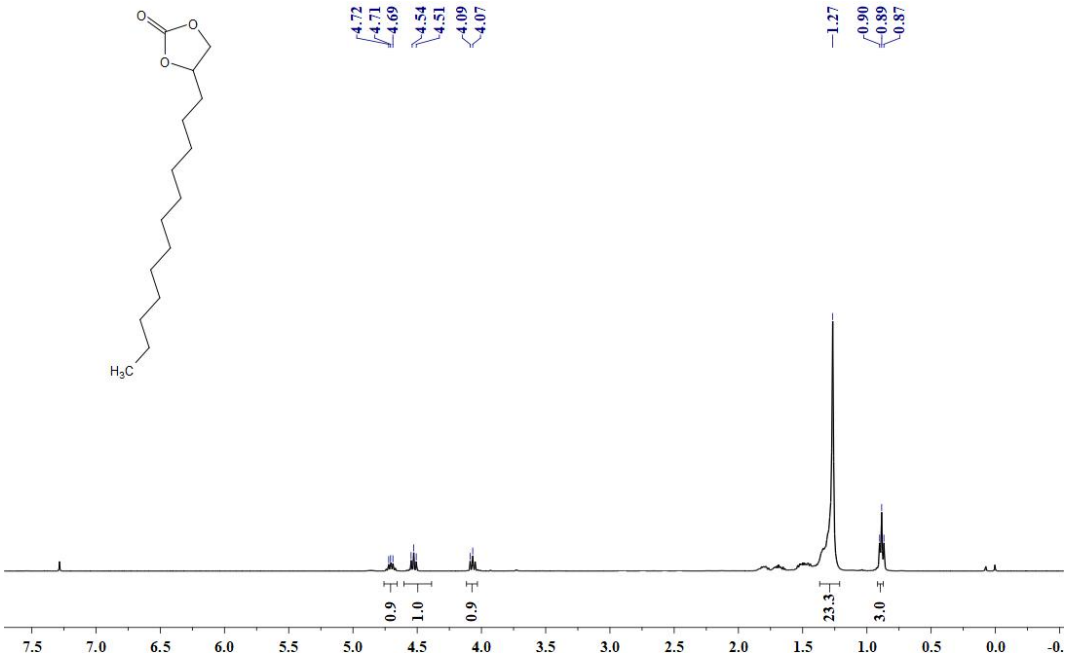

Supplementary Figure 14. ^{1}H NMR spectrum of 1,2-epoxytetradecane.

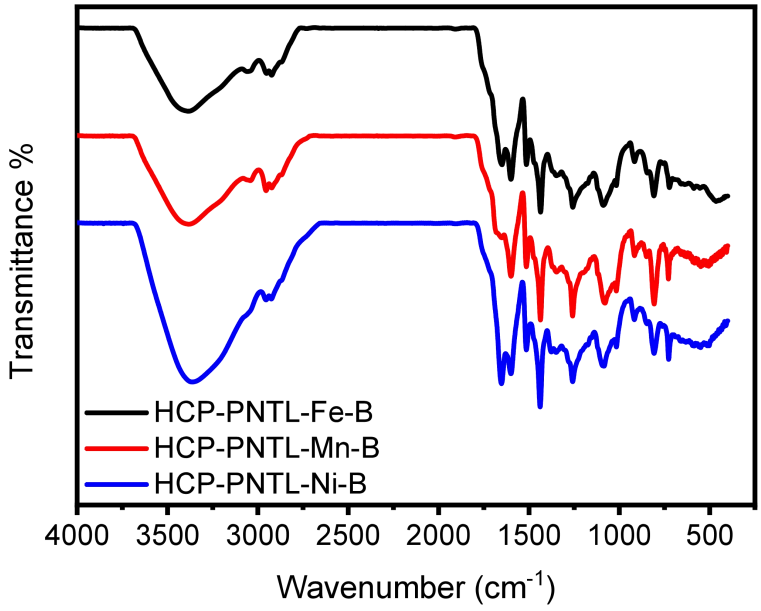

Supplementary Figure 15. FT-IR spectra of HCP-PNTL-M-B.

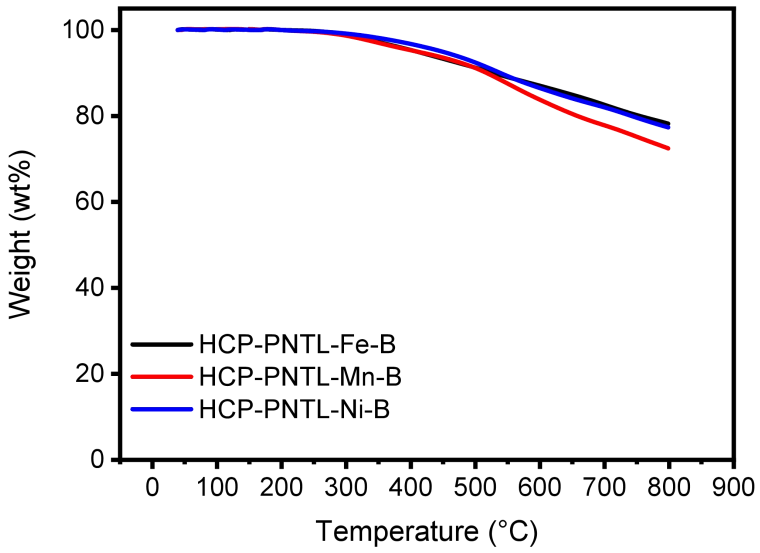

Supplementary Figure 16. TGA of HCP-PNTL-M-B (measured under N_2 atmosphere).

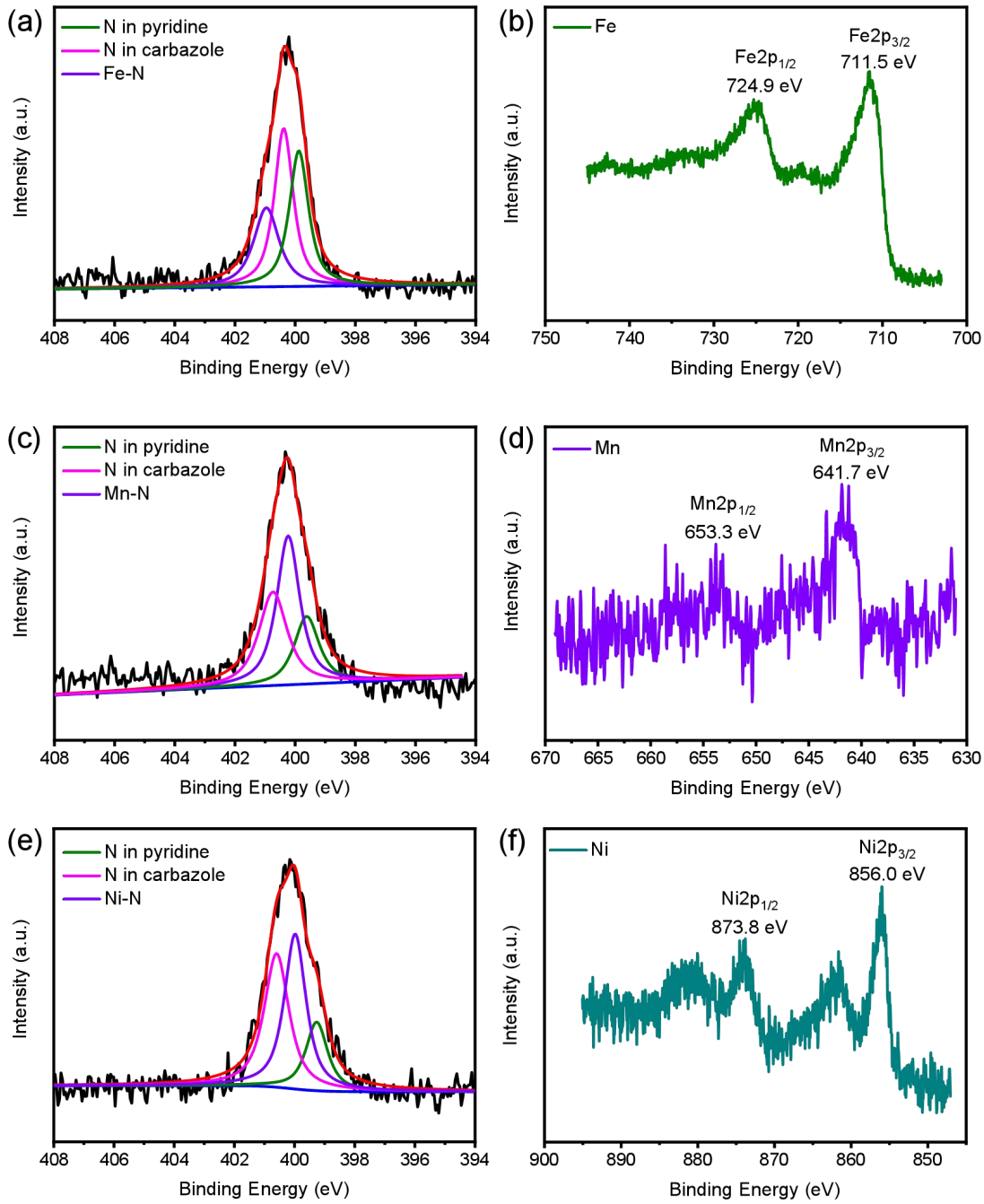

Supplementary Figure 17. XPS spectra for (a) N1s of HCP-PNTL-Fe-B, (b) Fe2p of HCP-PNTL-Fe-B, (c) N1s of HCP-PNTL-Mn-B, (d) Mn2p of HCP-PNTL-Mn-B, (e) N1s of HCP-PNTL-Ni-B and (f) Ni2p of HCP-PNTL-Ni-B.

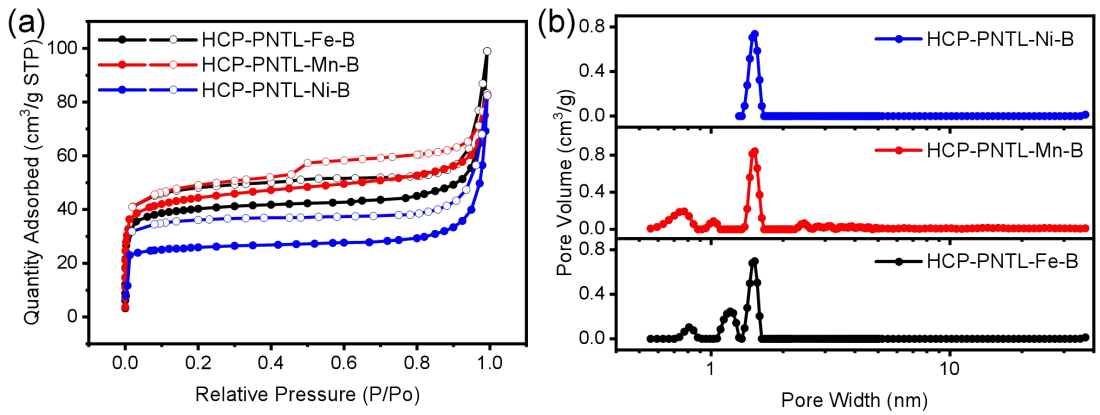

Supplementary Figure 18. (a) N_2 adsorption and desorption isotherms of HCP-PNTL-M-B; (b) Pore size distributions of HCP-PNTL-M-B.

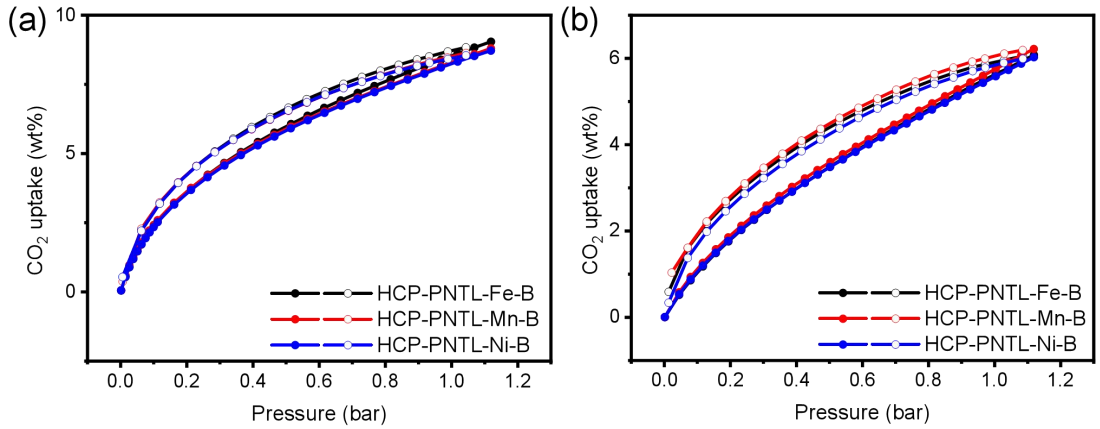

Supplementary Figure 19. CO_2 adsorption and desorption isotherms of HCP-PNTL-M-B at (a) 273.15 K and (b) 298.15 K.

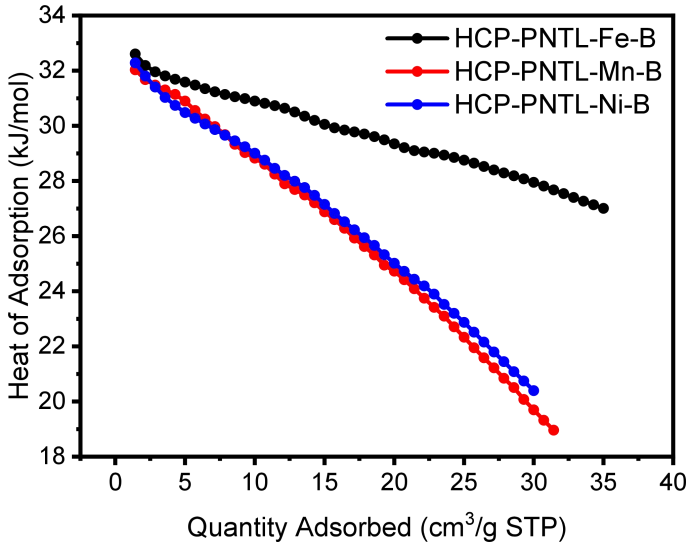

Supplementary Figure 20. Isotheric heat of adsorption for CO_2 of HCP-PNTL-M-B.

Supplementary Table 4. The performance comparison of HCP-PNTL-M-B with COFs and CTFs-based systems

Photocatalyst	Photosensitizer	Sacrificial agent	CO (μmol g^{-1} h^{-1})	Selectivity of CO	Ref.
Co@COF-TVBT-Bpy	$[Ru(bpy)_3]Cl_2$	TEOA	1133	49%	[15]
Co-FPy-CON	$(Ir[dF(CF_3)ppy]_2(dtbpy))PF_6$	TEOA	1683	76%	[16]
TFBD-COF-Co-SA	$[Ru(bpy)_3]Cl_2$	TEOA	1480	90%	[17]
DQTP-COF-Co	$[Ru(bpy)_3]Cl_2$	TEOA	1020	59%	[18]
H-COF-Ni	$[Ru(bpy)_3]Cl_2$	TEOA	2312	96%	[19]
Ni-PCD@TD-COF	$[Ru(bpy)_3]Cl_2$	TEOA	480	98%	[20]
Co-COFs	$[Ru(bpy)_3]Cl_2$	TEOA	2375	58%	[21]
Ni-COFs	$[Ru(bpy)_3]Cl_2$	TEOA	5310	95%	[21]
Fe-COFs	$[Ru(bpy)_3]Cl_2$	TEOA	1000	17%	[21]
Ni-TpBpy-COF	$[Ru(bpy)_3]Cl_2$	TEOA	966	96%	[22]
CTF-Bpy-Co	$[Ru(bpy)_3]Cl_2$	TEOA	1200	84%	[23]
Fe_2O_3@Por-CTF10	$[Ru(bpy)_3]Cl_2$	TEOA	400	93%	[24]
HCP-PNTL-Fe-B	$[Ru(bpy)_3]Cl_2$	TEOA	956	39%	This work
HCP-PNTL-Mn-B	$[Ru(bpy)_3]Cl_2$	TEOA	1480	71%	This work
HCP-PNTL-Ni-B	$[Ru(bpy)_3]Cl_2$	TEOA	2761	90%	This work
HCP-PNTL-Co-B	$[Ru(bpy)_3]Cl_2$	TEOA	2173	84%	This work

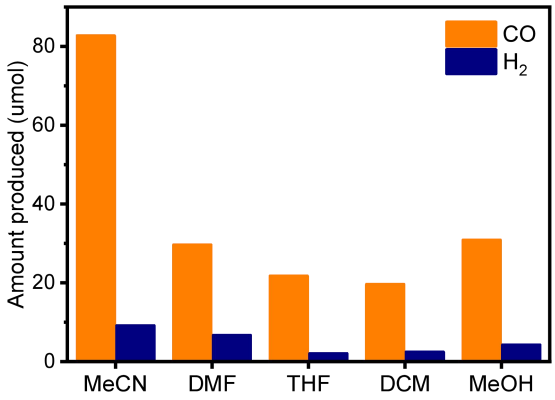

Supplementary Figure 21. Influence of solvent on the CO and H_2 production over HCP-PNTL-Ni-B.

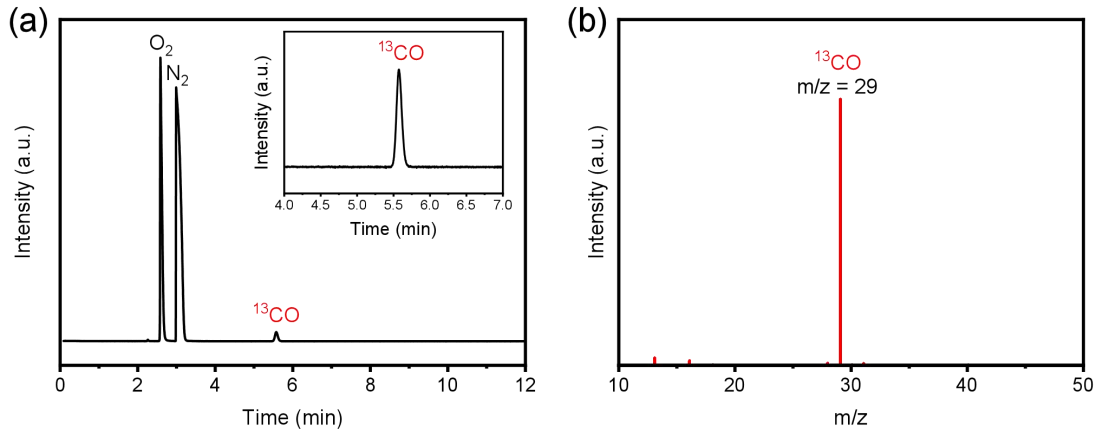

Supplementary Figure 22. GC-MS spectra of gas products after the photocatalytic reaction over HCP-PNTL-Ni-B; The isotopically labeled $^{13}CO_2$ was used as a substrate; (a) Total ion chromatogram; (b) GC-MS spectra of ^{13}CO peaks.

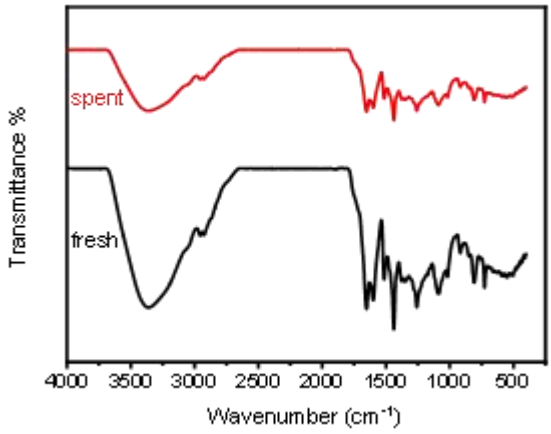

Supplementary Figure 23. FT-IR spectra of HCP-PNTL-Ni-B before and after CO_2 photoreduction reaction.

REFERENCES

1. Pu Y-J, Harding R E, Stevenson S G, et al. Solution processable phosphorescent rhenium(i) dendrimers. *J Mater Chem* 2007; 17: 4255-64. [DOI:10.1039/B707896J]

2. Ge Z, Hayakawa T, Ando S, et al. Synthesis and Properties of 3,8-Bis[4-(9H-carbazol-9-yl)phenyl]-1,10-phenanthroline for Phosphorescent OLEDs. *Chem Lett* 2008; 37: 262-63 [DOI:10.1246/cl.2008.262]

3. Chen J, Zhong M, Tao L, et al. The cooperation of porphyrin-based porous polymer and thermal-responsive ionic liquid for efficient CO2 cycloaddition reaction. *Green Chem* 2018; 20: 903-11 [DOI:10.1039/C7GC03801A]

4. Dai Z, Sun Q, Liu X, et al. Metalated porous porphyrin polymers as efficient heterogeneous catalysts for cycloaddition of epoxides with CO2 under ambient conditions. *J Catal* 2016; 338: 202-09 [DOI: 10.1016/j.jcat.2016.03.005]

5. Wang S, Song K, Zhang C, et al. A novel metalporphyrin-based microporous organic polymer with high CO2 uptake and efficient chemical conversion of CO2 under ambient conditions. *Journal of Materials Chemistry A* 2017; 5: 1509-15 [DOI:10.1039/C6TA08556C]

6. Dai Z, Sun Q, Liu X, et al. A Hierarchical Bipyridine-Constructed Framework for Highly Efficient Carbon Dioxide Capture and Catalytic Conversion. *ChemSusChem* 2017; 10: 1186-92 [DOI: 10.1002/cssc.201601375]

7. Puthiaraj P, Kim H S, Yu K, Ahn W S. Triphenylamine-based covalent imine framework for CO2 capture and catalytic conversion into cyclic carbonates. Microporous Mesoporous Mater 2020; 297: 110011 [DOI: 10.1016/j.micromeso.2020.110011]

8. Xie Y, Wang T T, Liu X H, Zou K, Deng W Q. Capture and conversion of CO2 at ambient conditions by a conjugated microporous polymer. *Nature Communications* 2013; 4: 1960 [DOI:10.1038/ncomms2960]

9. Wang W, Li C, Jin J, Yan L, Ding Y. Mg–porphyrin complex doped divinylbenzene based porous organic polymers (POPs) as highly efficient heterogeneous catalysts for the conversion of CO2 to cyclic carbonates. *Dalton Transactions* 2018; 47: 13135-41 [DOI:10.1039/C8DT02913J]

10. Sun Q, Aguila B, Perman J, Nguyen N, Ma S. Flexibility Matters: Cooperative Active Sites in Covalent Organic Framework and Threaded Ionic Polymer. *J Am Chem Soc* 2016; 138: 15790-96 [DOI:10.1021/jacs.6b10629]

11. Li H, Feng X, Shao P, et al. Synthesis of covalent organic frameworks via in situ

salen skeleton formation for catalytic applications. *Journal of Materials Chemistry A* 2019; 7: 5482-92 [DOI:10.1039/C8TA11058A]
12. Chun J, Kang S, Kang N, et al. Microporous organic networks bearing metal-salen species for mild CO2 fixation to cyclic carbonates. *Journal of Materials Chemistry A* 2013; 1: 5517-23 [DOI:10.1039/C3TA10477J]
13. Ji G, Yang Z, Zhang H, et al. Hierarchically Mesoporous o-Hydroxyazobenzene Polymers: Synthesis and Their Applications in CO2 Capture and Conversion. *Angew Chem* 2016; 128: 9837-41 [DOI:10.1002/anie.201602667]
14. Chen J, Li H, Zhong M, Yang Q. Hierarchical mesoporous organic polymer with an intercalated metal complex for the efficient synthesis of cyclic carbonates from flue gas. *Green Chem* 2016; 18: 6493-500 [DOI:10.1039/C6GC02367C]
15. Cui J X, Fu Y M, Meng B, et al. A novel cobalt-anchored covalent organic framework for photocatalytic conversion of CO 2 into widely adjustable syngas. *Journal of Materials Chemistry A* 2022; 10: 13418-27 [DOI: 10.1039/d2ta02648a]
16. Wang X, Fu Z, Zheng L, et al. Covalent organic framework nanosheets embedding single cobalt sites for photocatalytic reduction of carbon dioxide. *Chem Mater* 2020; 32: 9107-14 [DOI: 10.1021/acs.chemmater.0c01642]
17. Yang Y, Lu Y, Zhang H Y, et al. Decoration of Active Sites in Covalent–Organic Framework: An Effective Strategy of Building Efficient Photocatalysis for CO2 Reduction. *ACS Sustainable Chemistry & Engineering* 2021; 9: 13376-84 [DOI:10.1021/acssuschemeng.1c04994]
18. Lu M, Li Q, Liu J, et al. Installing earth-abundant metal active centers to covalent organic frameworks for efficient heterogeneous photocatalytic CO2 reduction. *Applied Catalysis B: Environmental* 2019; 254: 624-33 [DOI: 10.1016/j.apcatb.2019.05.033]
19. Yang S, Sa R, Zhong H, et al. Microenvironments enabled by covalent organic framework linkages for modulating active metal species in photocatalytic CO2 reduction. *Adv Funct Mater* 2022; 32: 2110694 [DOI: 10.1002/adfm.202110694]
20. Zhong H, Sa R, Lv H, et al. Covalent organic framework hosting metalloporphyrin-based carbon dots for visible-light-driven selective CO2 reduction. *Adv Funct Mater* 2020; 30: 2002654 [DOI: 10.1002/adfm.202002654]
21. Han B, Ou X, Zhong Z, et al. Rational Design of FeNi Bimetal Modified Covalent Organic Frameworks for Photoconversion of Anthropogenic CO2 into Widely Tunable Syngas. *Small* 2020; 16: 2002985 [DOI: 10.1002/smll.202002985]

22. Zhong W, Sa R, Li L, et al. A covalent organic framework bearing single Ni sites as a synergistic photocatalyst for selective photoreduction of CO2 to CO. *J Am Chem Soc* 2019; 141: 7615-21 [DOI: 10.1021/jacs.9b02997]
23. Hu X, Zheng L, Wang S, Wang X, Tan B. Integrating single Co sites into crystalline covalent triazine frameworks for photoreduction of CO 2. *Chem Commun* 2022; 58: 8121-24 [DOI: 10.1039/d2cc02481k]
24. Zhang S, Wang S, Guo L, et al. An artificial photosynthesis system comprising a covalent triazine framework as an electron relay facilitator for photochemical carbon dioxide reduction. *Journal of Materials Chemistry C* 2020; 8: 192-200 [DOI:10.1039/C9TC05297F]